System-level Modeling of a Micro Heat Pipe Fission Battery with Granular Pebble Bed Core: Steady-state Performance Evaluation

Kyeong Jun Park, Yelyn Ahn and Eung Soo Kim*
Department of Nuclear Engineering, Seoul National University
**Corresponding author: kes7741@snu.ac.kr*

1. Introduction

Heat pipe-based microreactors have attracted increasing attention as promising power sources for specialized missions, such as remote deployment, space exploration, and underwater operations, due to their structural simplicity, passive operation, and inherent stability [1]. While component-level studies on microreactors have been widely conducted, system-level analyses addressing coupled dynamics among the reactor core, heat pipes, and power conversion systems remain limited.

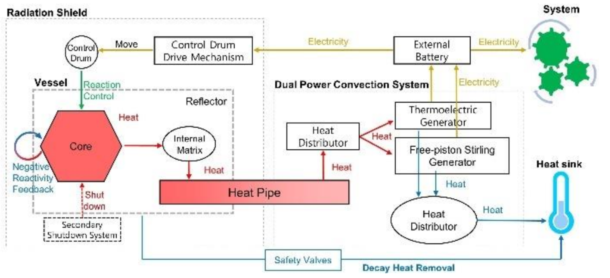

Fig 1. The schematic of the 20kWe Heat Pipe Fission Battery with Dual Power Conversion System

As shown in Figure 1, a previous study (Park et al., 2025) developed a system-level dynamic model of a 20 kWe micro fission battery with dual power conversion systems—a thermoelectric generator (TEG) and a free-piston Stirling generator (FPSG) operating in parallel—using the AMESim multi-domain simulation tool [2]. The prismatic core was modeled using thermal energy balance equations, and a thermal resistance approach was applied to the heat pipe model. The TEG model included the Thomson and Seebeck effects, while neutronics feedback used a point kinetics model. The nonlinear analysis model was applied to simulate the FPSG. The system demonstrated stable operation, producing 21.05 kWe at an overall efficiency of 29.4% as summarized in Table I., and achieved steady-state conditions within approximately 1,000 seconds. It maintained stability without external control during transients within a specific range, demonstrating its feasibility [2].

Table I. Design Specifications for 20 kWe Micro Fission Battery

Parameters	Value	Unit
Fuel Material	UN	
Matrix (Moderator) Material	Zr2H3	
Enrichment	11	%
Core Diameter	40	cm
Height of Active Core Zone	40	cm
Maximum Temperature of Fuel	1059	K
Core Thermal Power	74	kWt
Heat Pipe Material	Sodium	-
Number of Heat Pipes	37	EA
Heat Pipe Diameter	2	cm
Evaporation Section Length	40	cm
Evaporation Section Temperature	968	K
Condensation Section Temperature	953	K
TEG Condensation Section Length	70	cm
FPSG Condensation Section Length	50	cm
TEG Material	PbTe	-
Number of TE Elements	2,940	EA
Thermal Power Input	26.64	kWt
Electric Power Input	4.74	kWe
TEG Hot side Temperature	924.7	K
TEG cool side Temperature	334.8	K
Efficiency	17.8	%
FPSG type	β	-
Working Gas	He	-
Mean Pressure	70	Bar
FPSG Hot side Temperature	946.1	K
FPSG cool side Temperature	321.4	K
Displacer Piston Amplitude	4.66	Cm
Power Piston Amplitude	5.68	cm
Phase Difference	49.65	°
Alternator Resonant Frequency	34.48	Hz
Thermal Power Input	44.9	kWt
Electric Power Output	16.3	kWe

Building on this foundation, this study extends the system model by replacing the conventional hexagonal prismatic core with a granular pebble bed core and implementing a transient heat pipe model. These enhancements aim to improve the thermal stability and reliability of the core, while enabling the system model to simulate the entire operational process—including startup and shutdown—thereby expanding its capability as a simulation tool for analyzing microreactor system behavior.

Nomenclature

The Granular Pebble Bed Core

q'''	volumetric heat generation rate (W m^{-3})
D_{out}	outer diameter of i^{th} layer (m)
D_{in}	inner diameter of i^{th} layer (m)
h	height of the core (m)
$N_{HP,i}$	number of heat pipes of i^{th} layer
D_{HP}	diameter of heat pipe (m)
d_p	diameter of a pebble (m)
α_{mid}	packing fraction of pebbles in the bulk region

α_{HP}	packing fraction of pebbles within a half-particle distance from the heat pipe wall
α_{wall}	packing fraction of pebbles within a half-particle distance from the wall boundary
ρ_i	density of pebble bed cell i (kg m^{-3})
$C_{p,\,i}$	specific heat of pebble bed cell i (J Kg^{-1} K^{-1})
V_i	volume of pebble bed cell i (m^3)
T_i	temperature of pebble bed cell i (K)
q_v	volumetric heat generation rate of pebble bed (W m^{-3})
R_i	thermal resistance of pebble bed cell i (Ω)
T_w	temperature of wall (K)
r	core radius (m)
λ_{eff}	the effective thermal conductivity of pebble bed (W m^{-1} K^{-1})
q'''_b	volumetric heat transfer rate to pebble bed (W m^{-3})
q'''_w	volumetric heat transfer rate to wall (W m^{-3})
φ	void fraction of pebble bed
ε_r	pebble emissivity
σ	Stefan-Boltzmann constant (W m^{-2} K^{-4})
T	pebble temperature (K)
λ_f	thermal conductivity of fluid (W m^{-1} K^{-1})
λ_r	ratio between fluid & solid thermal conductivity
λ_s	thermal conductivity of solid (W m^{-1} K^{-1})
μ_p	poisson ratio
P_e	external pressure estimated by the weight of particles (N m^{-2})
E_s	Young modules (N m^{-2})
S_F	simple cubic arrangement constant ($S_F = 1$)
S	simple cubic arrangement constant ($S = 1$)
N_A	simple cubic arrangement constant ($1/4R^2$)
N_L	simple cubic arrangement constant ($1/2R$)

The Transient Heat Pipe

$\rho_{(i,\,j)}$	density of the cell (i, j) (Kg m^{-3})
$C_{p(i,j)}$	specific heat of the cell (i, j) (J Kg^{-1} K^{-1})
$V_{(i,j)}$	volume of the cell (i, j) (m^3)
$T_{(i,j)}$	temperature of the cell (i, j) (K)
$R_{(i,j)}$	thermal resistance of the cell (i, j) (Ω)
C_s	specific heat of solid (J Kg^{-1} K^{-1})
C_l	specific heat of liquid (J Kg^{-1} K^{-1})
H_{fus}	latent heat of fusion (J Kg^{-1})
T_m	melting temperature (K)
δT	temperature difference between the maximum solid temperature and the minimum liquid temperature (K)
T_{surf}	wick-vapor interface surface temperature (K)
R_{wi}	thermal resistance of wick (Ω)
R_{surf}	thermal resistance of wick-vapor surface (Ω)
R_{pc}	thermal resistance of phase change (Ω)
R_{rad}	thermal resistance of radiation (Ω)

The Thermoelectric Generator

j_i	current of section i (A)
ρ_i	density of section i (kg m^{-3})
V_i	volume of section i (m^{-3})
$Z\bar{T}$	dimensionless figure of merit
$\dot{W}_n$	electrical power output (W)
$\dot{Q}_h$	absorbed heat at warmer junction (W)
$\dot{Q}_c$	released heat at cooler junction (W)
n	number of thermoelectric elements
α	Seebeck coefficient (V K^{-1})
I	current (A)
T_h	temperature of warmer junction (K)
T_c	temperature of cooler junction (K)
R	resistance of thermoelectric element (Ω)
R_L	resistance of load resistance of TEG (Ω)

The Free-piston Stirling Generator

U	internal energy (W)
$\dot{m}_i$	mass flow rate of the cell i (kg s^{-1})
h_i	specific enthalpy of the cell i (J kg^{-1})
Q	heat (W)
W	work of the pressure forces (W)
M_d	mass of the Displacer Piston (D.P.) (kg)
x_d	displacement of the D.P. (m)
c_d	damping coefficient of the D.P. (N s m^{-1})
K_d	spring constant of the D.P. (N m^{-1})
F_d	pressure force between the expansion and compression cells (N)
M_p	mass of the Power Piston (P.P.) (kg)
x_p	displacement of the P.P. (m)
c_p	damping coefficient of the P.P. (N s m^{-1})
K_p	spring constant of the P.P. (N m^{-1})
F_p	pressure force between the compression and bounce cells (N)
F_e	induced electromotive force (N)
N	number of generator winding turns
ϕ	magnetic flux (Wb)
η_{mag}	generator magnetic efficiency
I_{alt}	generator current (A)
B	magnetic induction intensity of the linear generator (T)
L	coil length (m)
K_i	alternator current electromagnetic force constant (N A^{-1})
v_{emf}	induced voltage (V)
K_e	alternator constant (V s m^{-1})
R_{alt}	alternator resistance (Ω)
L_{alt}	alternator inductance (Ω)
C_t	tuning capacitance (μF)
R_{load}	external load resistance (Ω)
f	resonant frequency of the alternator (s^{-1})

2. Component Model Development

To advance the system model previously developed by Park et al. (2025), new component models were introduced while maintaining consistency in the system's input and output power. This approach ensures that the impact of the newly implemented models can be evaluated without altering the overall power balance of the microreactor system.

2.1 The Granular Pebble bed Core

To improve safety and simplicity, the core is being redesigned as a granular pebble bed from the prismatic core, enabling high-temperature operation, long refueling intervals, and passive shutdown.

Based on the heat balance of the previous study (Park et al., 2025), the reactor core thermal power was set to 74 kW. Referring to the volumetric heat generation rate of the HTR-PM reactor core [3], the pebble diameter was set to 1 cm to implement a granular-sized pebble bed. To ensure that each heat pipe of 2 cm diameter can transfer approximately 2 kW of thermal power to the power conversion system, a total of 37 heat pipes were arranged radially, as illustrated in Figure. 2.

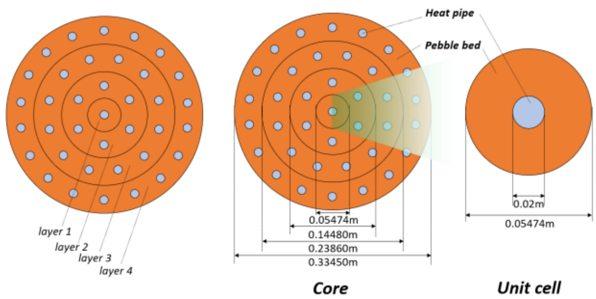

Fig 2. Calculation results of the granular core geometry

The following relations (1) and (2) were applied to calculate the core geometry.

$$q'''\left[\left\{\frac{\pi}{4}\left(D_{out,i}^2-D_{in,i}^2\right)h-N_{HP,i}\frac{\pi}{4}\left(D_{HP}+d_p\right)^2h\right\}\alpha_{mid}+\left\{N_{HP,i}\frac{\pi}{4}\left((D_{HP}+d_p)^2-D_{HP}^2\right)h\right\}\alpha_{HP}\right]=2N_{HP,i} \quad (1)$$

$$q'''\left[\frac{\pi}{4}\left(D_{out,i}^2-\left(D_{out,i}-d_p\right)^2\right)h\alpha_{wall}+\frac{\pi}{4}\left\{\left(\left(D_{out,i}-d_p\right)^2-D_{in,i}^2\right)-N_{HP,n}\left(D_{HP}+d_p\right)^2\right\}h\alpha_{mid}+N_{HP,n}\frac{\pi}{4}\left((D_{HP}+d_p)^2-D_{HP}^2\right)h\alpha_{HP}\right]=2N_{HP,i} \quad (2)$$

Heat transfer of the core was implemented as a 1D thermal network model (3) using the relation (4) based on the GAMMA+ 2.0 code [5] as shown in Figure 3.

$$\rho_i\, C_{p,i} V_i \frac{dT_i}{dt} = q_v V_i + \frac{T_{i-1}-T_i}{R_{(i-1,i)}} + \frac{T_i-T_{i+1}}{R_{(i,i+1)}} + \frac{T_{(i+1)}-T_{w(i+2)}}{R_{(i+1,i+2)}} \quad (3)$$

$$\rho C_p \frac{\partial T}{\partial t} = \frac{1}{r}\frac{\partial}{\partial r}\left(r\lambda_{eff}\frac{\partial T}{\partial r}\right) + q'''_b - q'''_w \quad (4)$$

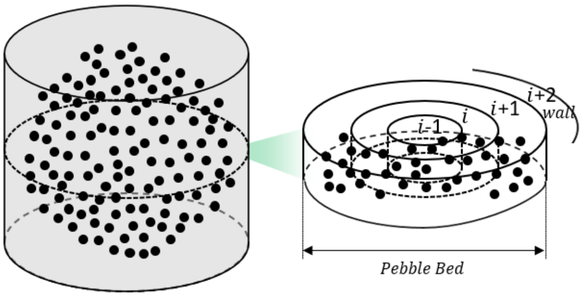

Fig 3. The Schematic of pebble bed core

The modified Zehner–Schlünder model is applied to calculate the effective thermal conductivity through the relations (5) – (8) [4], while convection is neglected because of the relatively small cylindrical geometry (⌀ 0.33 m × 0.34 m) and high operating temperature (> 900 K); this assumption is validated against SANA-I test data (IAEA-TECDOC-1163, 2000) by excluding the convection term from the effective thermal conductivity as shown in Figure 4.

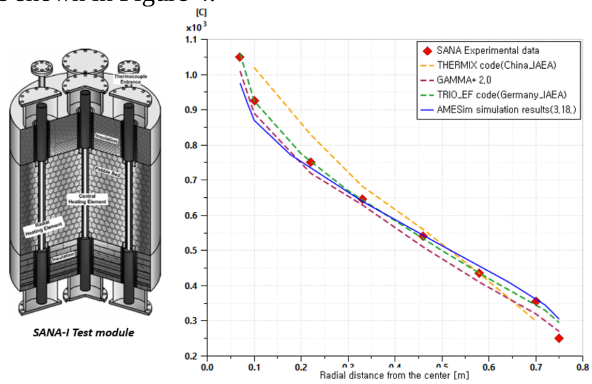

Fig 4. Validation results of the Heat Transfer model without convection

$$\lambda_{eff} = \lambda_{eff}^{void\_radiation} + \lambda_{eff}^{gas\_conduction} + \lambda_{eff}^{contact\_conduction} \quad (5)$$

$$\lambda_{eff}^{void\_radiation} = \left\{\left[1-\sqrt{1-\varphi}\right]\varphi + \frac{\sqrt{1-\varphi}}{(2/\varepsilon_r-1)}\frac{B+1}{B}\left[1+\frac{1}{(2/\varepsilon_r-1)\Lambda}\right]^{-1}\right\}4\sigma T^3 d_p \quad (6)$$

$$\lambda_{eff}^{gas\_conduction} = \lambda_f\left\{1-\sqrt{1-\varphi}+\frac{2\sqrt{1-\varphi}}{1-\lambda_r B}\left[\frac{(1-\lambda_r)B}{(1-\lambda_r B)^2}\ln\left(\frac{1}{\lambda_r B}\right)-\frac{B+1}{2}-\frac{B-1}{1-\lambda_r B}\right]\right\} \quad (7)$$

$$\lambda_{eff}^{contact\_conduction} = \lambda_s\left[\frac{3(1-\mu_p^2)}{4E_s}\frac{P_e S_F d_p}{2N_A}\right]^{\frac{1}{3}}\frac{1}{0.531S}\left(\frac{N_A}{N_L}\right) \quad (8)$$

$$B = 1.25\left(\frac{1-\varepsilon}{\varepsilon}\right)^{10/9}$$

$$\Lambda = \frac{\lambda_s}{4\sigma T^3 d_p}$$

2.2 The Transient Heat Pipe

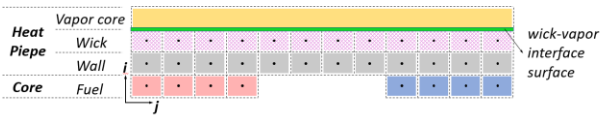

Fig 5. The Schematic of the Transient Heat Pipe model

As shown in Figure 5, the heat pipe model is being extended to a transient form by incorporating a solid–liquid phase change model and interfacial thermal resistance at the wick–vapor interface [6], through the equations (9) – (12).

$$\rho_{(i,j)}\, C_{p(i,j)} V_{i,j} \frac{dT_{i,j}}{dt} = \frac{T_{(i+1,j)}-T_{(i,j)}}{R_{(i+1,j)}} + \frac{T_{(i-1,j)}-T_{(i,j)}}{R_{(i-1,j)}} + \frac{T_{(i,j-1)}-T_{(i,j)}}{R_{(i,j-1)}} + \frac{T_{(i,j+1)}-T_{(i,j)}}{R_{(i,j+1)}} \quad (9)$$

$$C = \begin{cases} C_s & (T < T_m - \delta T) \\ \frac{H_{fus}}{2\delta T} + \frac{C_s + C_l}{2} & (T_m - \delta T \le T \le T_m + \delta T) \\ C_l & (T > T_m + \delta T) \end{cases} \quad (10)$$

$$T_{surf} = \frac{\frac{2T_{wi}}{R_{wi}} + \frac{T_v}{R_{surf}}}{\frac{2}{R_{wi}} + \frac{1}{R_{surf}}} \quad (11)$$

$$\frac{1}{R_{surf}} = \frac{1}{R_{pc}} + \frac{1}{R_{rad}} \quad (12)$$

2.3 The TEG

The modeling of the TEG was conducted by integrating the thermal energy conservation equation with the Thomson and Seebeck effects [7]. The heat transfer in a thermoelectric element is expressed by Equation (13), which incorporates Joule heating resulting from electric current flow.

$$M_i C_{pi} \frac{dT_i}{dt} = \sum_j \frac{T_j - T_i}{R_{ij}} + {j_i}^2 \rho_i V_i \quad (13)$$

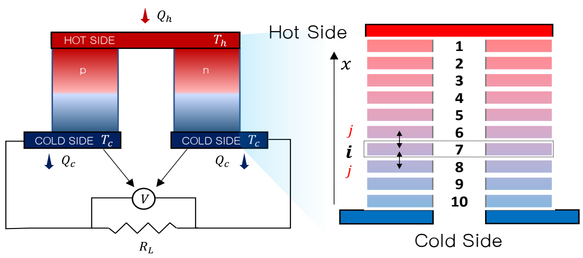

Fig 6. The Schematic of the TEG model

The net power output of the TEG is governed by the difference between the heat absorbed at the hot junction and the heat rejected at the cold junction, as described in Equation (14) with the thermoelectric effect considered [7]. Equation (15) defines the conversion efficiency, where $Z\overline{T}$ is the dimensionless figure of merit, a key indicator for evaluating thermoelectric performance.

$$\dot{W}_n = \dot{Q}_h - \dot{Q}_c = n[\alpha I(T_h - T_c) - I^2 R] = nI^2 R_L \quad (14)$$

$$\eta_{th} = \frac{\left(1-\frac{T_c}{T_h}\right)\frac{R_L}{R}}{\left(1-\frac{R_L}{R}\right) - \frac{1}{2}\left(1-\frac{T_c}{T_h}\right) + \frac{1}{2Z\overline{T}}\left(1-\frac{R_L}{R}\right)^2\left(1+\frac{T_c}{T_h}\right)} \quad (15)$$

2.4 The FPSG

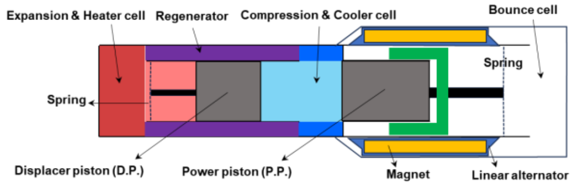

Fig 7. The Schematic of the FPSG model

As shown in Figure 7, the FPSG has been advanced from the traditional Stirling cycle through the elimination of mechanical drive components and the introduction of a free piston system, thereby enhancing its power output via pressurization [8]. In this research, a nonlinear approach is adopted for accurate modeling, incorporating a simplified representation of the alternator system and electrical circuits [9,10]. To implement this model, the FPSG is divided into three domains—thermal & fluidic, piston mechanical, and electrical—for calculation.

To implement the thermal and fluidic domain of the FPSG, the fundamental energy conservation equations (16) are applied. Using the initial values assigned to each cell, the variations in mass and temperature across the cells are calculated.

$$\frac{dU}{dt} = \sum \dot{m}_i h_i + \frac{dQ}{dt} + \frac{dW}{dt} \quad (16)$$

In the piston's mechanical domain, the applied force—accounting for pressure fluctuations and the induced electromotive force—is evaluated using the fundamental equation of motion. This enables the determination of the piston's displacement and velocity [11]. The governing equations for the displacer and power pistons are given in:

$$M_d \ddot{x_d} + c_d \dot{x_d} + K_d x_d = F_d \quad (17)$$

$$M_p \ddot{x_p} + c_p \dot{x_p} + K_p x_p = F_p + F_e \quad (18)$$

To implement the electrical domain, it is essential to account for the force exerted on the power piston by the induced electromotive force, which is determined by the piston's velocity. This effect is evaluated using a simplified alternator analysis model [12]. Furthermore, the generator parameters must be carefully designed to achieve resonance with the engine [13]. The induced electromotive force of the alternator is calculated as follows:

$$F_e = N \frac{d\phi}{dx_p} \eta_{mag} I_{alt} = BLI_{alt} = K_i I_{alt} \quad (19)$$

$$v_{emf} = K_e \cdot \dot{x_p}, \text{ where } K_e = N \frac{d\phi}{dx_p} \quad (20)$$

$$v_{emf} = v_{R_{alt}} + v_{L_{alt}} + v_{C_t} + v_{R_{load}} \quad (21)$$

$$\frac{dI_{alt}}{dt} = \frac{K_e}{L_{alt}}\dot{x}_p - \frac{R_{alt}+R_{load}}{L_{alt}}I_{alt} - \frac{1}{L_{alt}}v_{C_t} \quad (22)$$

$$\frac{dv_{C_t}}{dt} = \frac{1}{C_t}I_{alt} \quad (23)$$

$$\frac{1}{2\pi\sqrt{L_{alt}C_t}} = f \quad (24)$$

3. System Integration and Simulation

3.1 System Integration

To integrate the individual component models into a system model, the system design was established as shown in Table II. First, the maximum core and pebble temperatures of proven pebble bed reactors were reviewed, and the maximum pebble temperature of the present model was set accordingly (HTR-PM 1055 ℃, PMBR 1050 ℃), while also considering the general design limit of 1600 ℃ reported in the literature [14, 15]. Based on this temperature, the design criteria of heat pipes capable of transferring the required heat were examined, and the working fluid and design parameters were determined [16].

Under these conditions, the design parameters of the TEG and FPSG were adjusted to ensure that the system could achieve an efficiency of at least 20%. In this configuration, each heat pipe was designed to transfer about 2 kW of heat by setting the evaporator length to 0.34 m and the contact area to 0.02136 m², while the condenser lengths were allocated as 0.4 m for the TEG hot side and 0.5 m for the FPSG heater head to enable sufficient heat transfer at the condenser section. Furthermore, compared to the previous model, the operating conditions were shifted to higher temperatures, and the power conversion system was configured in parallel with two FPSGs and one TEG to ensure a minimum system efficiency of over 20%

Table II. Design Parameters for Steady-state Simulation

Parameters	**Value**	**Unit**
Fuel Material	TRISO	-
Pebble diameter	1	cm
Matrix (Moderator) Material	Graphite	-
Enrichment	11	%
Core Diameter	33.45	cm
Height of Active Core Zone	34	cm
Maximum Temperature of Pebble	1040	℃
Volumetric Core Power Density	5.305	MW/m^3
Packing fraction of Pebble	0.59	-
Core Thermal Power	74	kWt
Heat Pipe Material	Sodium	-
Number of Heat Pipes	37	EA
Heat Pipe Diameter	2	cm
Evaporation Section Length	40	cm
Evaporation Section Temperature	950	℃
Condensation Section Temperature	930	℃
Heat Transfer Performance	2	kW
TEG Condensation Section Length	40	cm
FPSG Condensation Section Length	50	cm
TEG Material	PbTe	-
Number of TE Elements	2,940	EA
Thermal Power Input	30	kWt
Electric Power Input	5	kWe
TEG Hot side Temperature	935	℃
TEG cool side Temperature	330	℃
Efficiency	16.6	%
FPSG type	β	-
Working Gas	He	-
Mean Pressure	70	Bar
FPSG Hot side Temperature	935	℃
FPSG cool side Temperature	305	℃
Displacer Piston Amplitude	3.3	cm
Power Piston Amplitude	3.55	cm
Phase Difference	49.65	°
Alternator Resonant Frequency	34.48	Hz
Thermal Power Input	22	kWt
Electric Power Output	6	kWe
Efficiency	27.2	%

3.2 Steady-state Simulation Results

Based on the established design, a steady-state simulation was conducted to evaluate the feasibility of the proposed system. As shown in Figure 8 and Table III, the results indicated that the reactor core with a total thermal output of 74.29 kWth could maintain the maximum pebble temperature at 1044.56 ℃, which is well below the design limit of 1600 ℃ for pebble bed reactors and consistent with the reported maximum pebble temperatures of demonstrated systems such as HTR-PM (1055 ℃) and PBMR (1050 ℃).

Table III. Steady-state Simulation Results

Variables	**Value**	**Unit**
System Thermal Power Input	74.29	kWt
System Electrical Power Output	16.18	kWe
Efficiency	21.78	%
Maximum Temperature of TRISO particle	1046.55	℃
Maximum Temperature of Pebble	1044.56	℃
Mean Temperature of Unit Core	1018.58	℃
Core Thermal Power	74.29	kWt
Heat Pipe Heat transfer performance	2.008	kW
Evaporation Section Temperature	940.44	℃
Condensation Section Temperature	930.20	℃
TEG Material	PbTe	-
Number of TE Elements	2,940	EA
Thermal Power Input	29.21	kWt
Electric Power Input	4.4	kWe
TEG Hot side Temperature	930.2	℃
TEG cool side Temperature	335.2	℃
Efficiency	15.06	%
FPSG Hot side Temperature	926.2	℃
FPSG cool side Temperature	302.8	℃
Displacer Piston Amplitude	3.39	cm
Power Piston Amplitude	3.42	cm

Phase Difference	49.65	°
Alternator Resonant Frequency	34.48	Hz
Thermal Power Input	22.55	kWt
Electric Power Output	5.89	kWe
Efficiency	26.1	%

Each heat pipe transferred approximately 2.008 kW of heat to the power conversion units, ensuring stable thermal transport within material constraints. In the power conversion system, the dual FPSGs and single TEG operated in a complementary manner, leading to an overall electrical efficiency of over 20%.

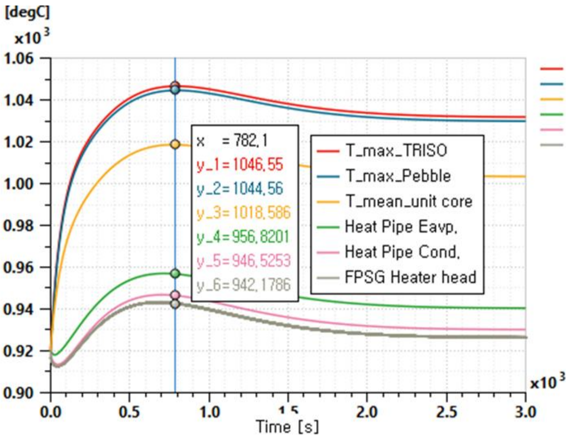

(a) Core and Heat pipe Temperature distribution

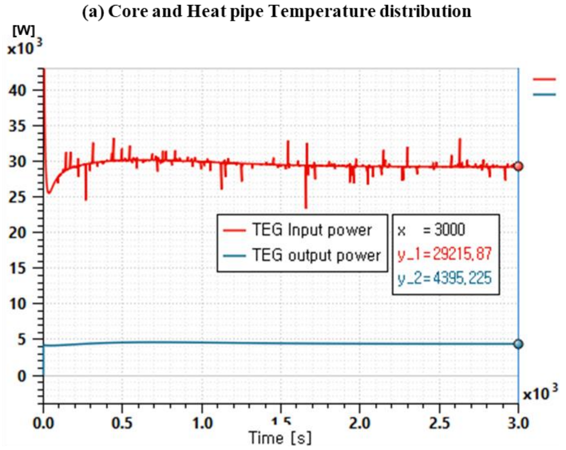

(b) TEG Input and Output power

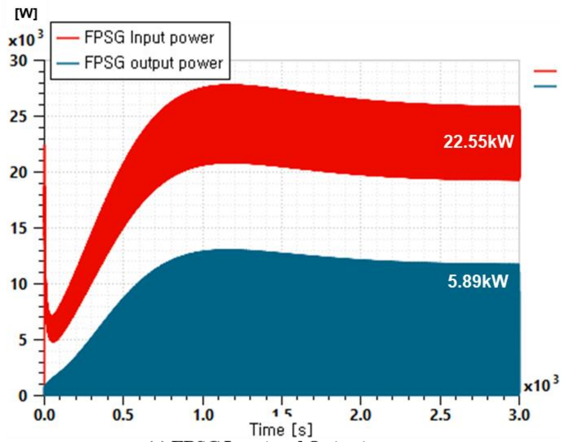

(c) FPSG Input and Output power

Fig 8. Behavior of key variables of the System

4. Summary & Conclusion

In this study, building upon the previous model by Park et al. (2025), the prismatic-core-based micro heat pipe reactor system model was extended by replacing the core model with a granular pebble bed core and improving the heat pipe model into a transient heat pipe model.

The steady-state analysis results showed that under a total thermal output of 74.29 kWth, the maximum temperature of the TRISO particle was maintained at 1046.55 ℃ and that of the pebble at 1044.56 ℃, remaining well below the design limit of 1600 ℃ reported in the literature and consistent with the operating ranges of demonstrated high-temperature gas-cooled reactors (HTR-PM: 1055 ℃, PBMR: 1050 ℃). Each heat pipe transferred approximately 2.008 kW of heat in a stable manner without exceeding material constraints. In addition, the dual FPSGs and single TEG in the power conversion system operated in a complementary manner, achieving efficiencies of 26.1% and 15.06%, respectively, which yielded an overall system efficiency of 21.78% and a net electrical output of 16.18 kWe.

These results demonstrate that the proposed system configuration not only satisfies thermal design requirements but also ensures stable power conversion performance. Furthermore, the improved system model can serve as a valuable foundation for future applications, including transient analysis, long-term operational reliability assessment, and adaptability studies under diverse mission environments.

Acknowledgement

This work was supported by the National Research Foundation of Korea (NRF) grant funded by the Korea government (MSIT) (No. RS-2024-00436693).

REFERENCES

[1] R. Testoni, A. Bersano, S. Segantin, Review of nuclear microreactors: Status, potentialities and challenges, Prog. Nucl. Energy 138 (2021) 103822.

[2] Park, Kyeong Jun, Eung Soo Kim, and Young Beom Jo. "Development of dynamic simulation model for 20 kWe micro heat pipe fission battery with dual power conversion system." Applied Thermal Engineering 258 (2025): 124505.

[3] Zhang, Zuoyi, et al. "Current status and technical description of Chinese 2× 250 MWth HTR-PM demonstration plant." Nuclear Engineering and Design 239.7 (2009): 1212-1219.

[4] Niessen, H. F., and S. Ball, eds. Heat transport and afterheat removal for gas cooled reactors under accident conditions. IAEA, 2000.

[5] H. S. Lim, "GAMMA+2.0 Volume II: Theory Manual," KAERI/TR8662/2021, Korea Atomic Energy Research Institute (2021).

[6] Kim, Ye Sung, and Hyoung Kyu Cho San Lee. "Implementation of Start-up/Shutdown Model into Alkali Metal Heat Pipe Analysis Code."

[7] Lee, H. (2016). Thermoelectrics: design and materials. John Wiley & Sons.

[8] Thombare, D.G.; Verma, S.K. Technological development in the Stirling cycle engines. Renew. Sustain. Energy Rev. 2008, 12, 1–38.

[9] Zare SH, Tavakolpour-Saleh AR. Nonlinear dynamic analysis of solar free piston hot-air engine. Modares Mech Eng. 2015;15(9): 223-234.

[10] Benvenuto, G., and F. De Monte. "Analysis of free-piston Stirling engine/linear alternator systems. Part I-Theory." Journal of propulsion and power 11.5 (1995): 1036-1046.

[11] Li, Huaqi, et al. "Development of a performance analysis model for free-piston stirling power convertor in space nuclear reactor power systems." Energies 15.3 (2022): 915.

[12] G. Benvenuto, F. De Monte, Analysis of free-piston Stirling engine/linear alternator systems. Part I-Theory, J. Propul. Power 11 (5) (1995) 1036–1046.

[13] Z. Jia, et al., Study on the coupling between engine and alternator in a free-piston Stirling generator, Appl. Therm. Eng. 217 (2022) 119222.

[14] Sun, Qi, et al. "A review of HTGR graphite dust transport research." Nuclear Engineering and Design 360 (2020): 110477.

[15] Zhang, Zuoyi, et al. "Design aspects of the Chinese modular high-temperature gas-cooled reactor HTR-PM." Nuclear Engineering and Design 236.5-6 (2006): 485-490.

[16] Peterson, G. P. (1994). An introduction to heat pipes. Modeling, testing, and applications. Wiley Series in Thermal Management of Microelectronic and Electronic Systems.